Space-Time Spectral Analyses of Northern Hemisphere Geopotential Heights

PETER SPETH[1] AND ROLAND A. MADDEN

National Center for Atmospheric Research,[2] Boulder, CO 80307

(Manuscript received 16 August 1982, in final form 30 December 1982)

ABSTRACT

A space-time spectral analysis of a long time series of observed geopotential heights for each season at several levels and latitudes of the Northern Hemisphere was performed as part of a continuing investigation of large-scale traveling waves. The data set that is analyzed consists of the first six zonal wavenumbers. A discussion emphasizes westward traveling wave 1 with periods near 16 and 5 days which we argue are consistent with external Rossby waves. An additional outstanding feature is an eastward propagating wave 6 which may result from baroclinic instability.

1. Introduction

There is considerable observational evidence that traveling, large-scale (zonal wavenumbers 1–3) wave-like disturbances are regular features of the atmosphere. Because these disturbances can have relatively large amplitudes, it is important to establish as much as possible about their nature so that we may better understand time variations in the large-scale circulation. Wavenumber–frequency and space–time spectral analyses have been used successfully to analyze model data (e.g., Hayashi, 1974; Tsay, 1974; Hayashi and Golder, 1977) and in observational studies of waves (*e.g.*, Kao, 1970; Pratt and Wallace, 1976; Kao and Chi, 1978; Fraedrich and Böttger, 1978; Schäfer, 1979; Zangvil and Yanai, 1980a,b; Speth and Kirk, 1981). Here, we perform space–time spectral analyses of a long time series of observed geopotential heights as part of a continuing investigation aimed at further establishing their typical periods and structures.

What is known about the largest of these wave-like disturbances is reasonably consistent with theoretical predictions of external Rossby waves or waves of the second class. The so-called waves of the second class are free or normal modes of certain simple atmospheric models whose horizontal structures are given by Hough functions (Margules, 1893; Hough, 1898; Haurwitz, 1937). The frequencies and structures depend on the rotation of the earth and on an equivalent or, in the case of constant density, the actual depth of the fluid (*e.g.*, Lamb, 1932; Longuet-Higgins, 1968; Holton, 1975). The equivalent depth of an isothermal atmosphere is ~10 km and the vertical structure of the waves of the second class is that of a Lamb wave [Lamb, 1932, Eq. (1), Article 311a]. Although the energy density decreases exponentially with height, the amplitude a of the wave increases upward according to

$$\ln a(p) = \kappa \ln(p_0/p) + \ln a(p_0), \qquad (1)$$

where $\kappa = (\gamma - 1)/\gamma$, γ is the ratio of specific heats, p is the pressure, and p_0 is some reference pressure.

Rossby–Haurwitz waves are the β-plane and/or non-divergent approximations of the waves of the second class (Rossby *et al.*, 1939; Haurwitz, 1940a,b). Rossby referred to them as planetary waves ". . . whose shape, wavelength and displacement are controlled by the variation of the Coriolis parameter with latitude" (Rossby, 1949). Geisler and Dickinson (1975) call waves of the second class with vertical structures similar to the Lamb wave "external Rossby waves." In the absence of background winds they move westward relative to a point on earth. Unfortunately, neither the existence nor the frequencies and structures of analogous waves of the second class in the real atmosphere can be theoretically predicted with certainty. Inclusion of realistic background winds, for example, make the separation of vertical and horizontal dependence and, as a result, analytical solution impossible. Despite the difficulties in making perfectly realistic simulations, the results of recent numerical studies of traveling waves of the second class are consistent with observations and support the conclusion that the observed disturbances are indeed their atmospheric counterparts. For example, studies of the generation of traveling waves in numerical models suggest that their source of energy is random forcings which excite free modes of models in certain preferred frequency bands (Hirota, 1971a,b; Schoeberl and Clark, 1980; Salby, 1981a,b; Garcia and

[1] Permanent affiliation: Institut für Geophysik und Meteorologie, Kerpener Str. 13, D-5000 Köln 41, Federal Republic of Germany.

[2] The National Center for Atmospheric Research is sponsored by the National Science Foundation.

Geisler, 1981). In addition, even in the presence of realistic background winds the structures of the excited model waves are, at least in the troposphere, similar to those predicted by the simpler theoretical treatments of the external Rossby wave. This result is apparently independent of the structure of the forcing itself (Geisler and Dickinson, 1976; Salby, 1981a,b).

A summary follows of space–time spectra of zonal wavenumbers one through six computed for several tropospheric and stratospheric levels, several Northern Hemisphere latitudes, and for each season. Some limited comparisons between what can be learned from the spectra and simple model predictions of the largest scale (zonal wavenumber one) external Rossby waves are made. In addition, we comment on eastward propagating variance that is particularly marked for wavenumber 6. This variance is probably a manifestation of disturbance already reported and related to waves generated by baroclinic or barotropic instabilities. The space–time spectral technique is presented in Section 2 along with a description of the data. The resulting frequency spectra of the first six zonal wavenumbers are summarized for each season separately in Section 3. These results are discussed further in Section 4. Finally, an overall summary and outlook is contained in Section 5.

2. Computational procedures and data

In this paper, the space–time spectral analysis is applied (Pratt, 1976; Hayashi, 1977). If geopotential height H as a function of longitude λ (positive to the east) and time t is expanded in zonal Fourier harmonics of wavenumber k,

$$H(\lambda, t) = [H(\lambda, t)] + \sum_{k=1}^{\infty} \{c_k(t) \cos(k\lambda) + s_k(t) \sin(k\lambda)\}. \quad (2)$$

Then the space–time power spectrum of progressive (+) and retrogressive (−) waves P may be computed by the formula

$$P(k, \pm n) = \tfrac{1}{4}[P_n(c_k) + P_n(s_k) \pm 2Q_n(c_k, s_k)], \quad (3)$$

where n is the normalized time frequency, P_n are the time–power spectra and Q_n the quadrature spectrum of c_k and s_k. A positive frequency designates an eastward traveling wave. The space–time power spectrum of the standing oscillation ST is expressed as:

$$\mathrm{ST}(k, |n|) = \{\tfrac{1}{4}[P_n(c_k) - P_n(s_k)]^2 + K_n^2(c_k, s_k)\}^{1/2}, \quad (4)$$

where K_n is the co-spectrum.

With (3) and (4), it is possible to isolate the "pure" progressive and retrogressive parts PPUR of a wave

$$\mathrm{PPUR}(k, \pm n) = P(k, \pm n) - \tfrac{1}{2}\mathrm{ST}(k, |n|). \quad (5)$$

We computed (5) for geopotential height, and we will abbreviate (5) as being the power of eastward or westward traveling waves.

This method of partitioning space–time power spectra into standing and traveling wave parts is based on the following definitions and assumptions (Hayashi, 1982):

1) Standing waves are defined as consisting of eastward and westward moving components which are of equal amplitude and are coherent.
2) Traveling waves are defined as consisting of eastward and westward moving components which are incoherent with each other.
3) It is assumed that standing waves and traveling waves are of a different origin and are incoherent with each other.

Grid point values of geopotential height and temperature at 13 levels (850, 700, 500, 400, 300, 250, 200, 150, 100, 70, 50, 30, 10 mb) were available. They were taken from daily 1200 GMT analyses made by the National Meteorological Center (NMC). More general information about the data sets is given by Jenne (1975). The data were first interpolated from the NMC octagon to a 5° × 10° latitude–longitude grid. Harmonic analyses determining the first six zonal wavenumbers was then performed with a latitudinal spacing of 10° between 20 and 80°N. Data for the period 1 January 1964 through 31 December 1980 were available. These data were broken up into 17 spring, summer and autumn segments and 16 winter segments. Exceptions are levels 400, 250 and 70 mb, where the following number of data segments was available:

	Spring	Summer	Autumn	Winter
70 mb	11	12	12	11
250 mb	15	16	16	15
400 mb	15	16	16	15

Spring starts on 1 March, summer on 1 June, autumn on 1 September, and winter on 1 December. Each season is defined to last for 96 days. The slight overlapping of seasons allowed for some saving of computer time when computing Fourier transforms.

From the resulting time series of the cosine and sine coefficients of waves 1 to 6 [Eq. (1): $c_k(t)$ and $s_k(t)$, $k = 1, \ldots, 6$] a Fast Fourier Transform routine was used to compute power spectra, co- and quadrature spectra for each latitude and level. From these in turn the space–time power spectra of the traveling wave components were estimated [Eq. (5)] Linear trends and the 96-day averages were removed from the time series and five values were tapered to zero at each of their ends. A running average over three adjacent values was applied to each spectral estimate

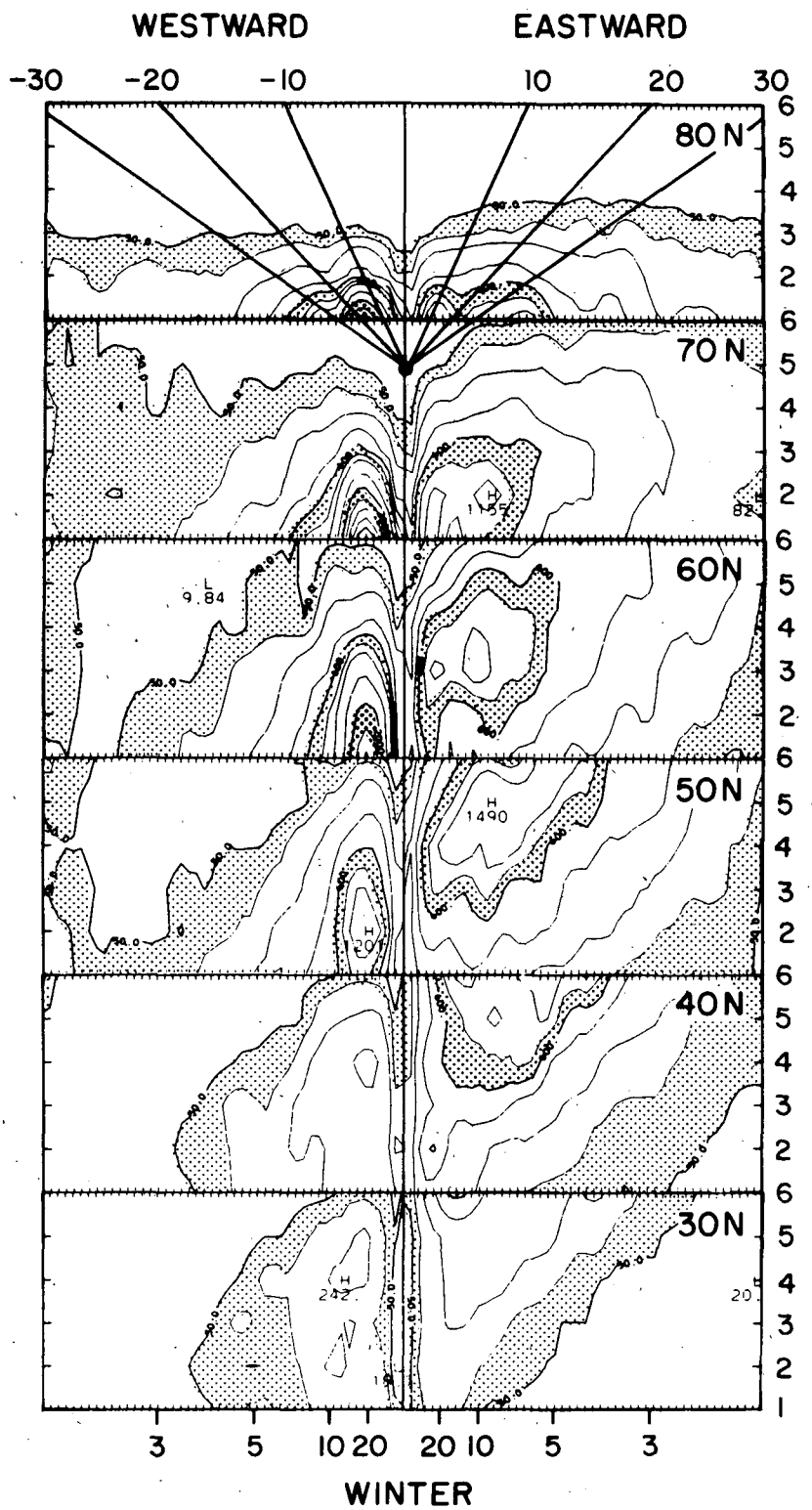

FIG. 1. Power of traveling waves of geopotential height for winter at 250 mb. The ordinates give wavenumbers (k) and the small tick marks along the abscissas represent integer values of n for the frequencies $n/96$ days, $n = \pm 1, \ldots, \pm 47$. Periods in days are indicated along the lower abscissa. The heavy slanting lines in the top panel (80°N) indicate lines of equal phase velocity in degrees longitude/day (along upper abscissa) which converge at $k = 0$ and zero frequency, to the point which is marked by a dot in the second panel from the top.

of power spectra, co- and quadrature spectra with a resulting frequency resolution of 3/96 days.

3. Results

From vertical cross sections (not shown here) we found that the largest variance exists in levels between 300 and 150 mb and additionally, for some latitudes and wavenumbers, at 10 mb. In the latter case, the variance increases in general monotonically from the lower troposphere to 10 mb. We have selected the results from the 250 mb level in order to illustrate many of the essential features of the space time spectra without reproducing results from all levels.

The discussion of results concentrates on two topics:

1) An overview of the dependence of the propagating variance on latitude, season and wavenumber is discussed qualitatively with the aid of wavenumber frequency spectra in Section 3a.

2) Some details are discussed with the aid of frequency spectra for discrete wavenumbers in Section 3b. This discussion emphasizes some outstanding features: namely those that relate to the westward traveling wave-1 with periods near 16 and five days and eastward traveling wave 6. In addition, we have included the spectra for all wave numbers because we feel that they may be of value for future investigations.

a. Wavenumber frequency spectra

The wavenumber frequency spectra of geopotential height for winter and 250 mb are given in Fig. 1. With the understanding that by "low frequencies" and "intermediate frequencies," i.e., periods longer than 12 days and between three and 12 days respectively, the following general features can be seen. The diagrams for 50, 60 and 70°N show that for low frequency westward traveling (wave-1 and wave-2) clear maxima exist, which far exceed those in the same period range of eastward traveling waves. At 80°N, distinct maxima are found only for $k = 1$ and the largest power is connected with the westward traveling wave. In that latitude wavenumbers higher than 1 can be neglected. This is, at least in part, to be expected as a consequence of the spherical geometry of the earth.

In contrast, for latitudes 20 (not shown), 30 and 40°N the largest amount of power is concentrated in eastward traveling wave 6 (possibly higher wavenumbers as well) at both low and intermediate frequencies. Proceeding farther to the north, the peaks of eastward traveling waves shift to lower wavenumbers: $k = 5$ at 50°N, $k = 4$ and $k = 3$ at 60°N, $k = 2$ at 70°N, and finally $k = 1$ at 80°N.

Fig. 2 shows the wavenumber frequency spectra of geopotential height for spring. The diagrams reveal in general the same features as those for winter, however, the power of all waves is reduced.

The wavenumber frequency spectra for summer are given in Fig. 3. Some features are seen which are different from winter and spring. At 30°N, westward propagating variance is largest, and the nearly vertical orientation of contour lines indicates that the spectra for each westward traveling wave, 1 through 6, are similar. Compared to winter at 40 and 50°N, the maximum variance for westward traveling waves is now connected with shorter waves ($k = 5$ at 40°N, and $k = 4$ at 50°N). For latitudes north of 60°N, the shape of the spectra of westward traveling waves is essentially the same as in winter and spring. North of 40°N, the maxima in the variance of eastward traveling waves have shifted to higher wavenumbers as compared to those of winter and spring ($k = 6$ at 50°N, between $k = 3$ and $k = 6$ at 60°N, $k = 3$ at 70°N). At 80°N, the eastward traveling wave-1 variance is larger than that in spring and, in fact, is comparable in magnitude to that of winter.

In autumn (Fig. 4), intermediate frequency eastward traveling waves between 50 and 80°N have variance much larger than that in spring and summer and comparable to, or larger than (50 and 60°N), that of winter. For 50 and 60°N, the variance connected with eastward traveling waves is much larger than that connected with westward traveling waves, in contrast to similar comparisons in other seasons.

Some of these features are summarized with the aid of Fig. 5. For winter and lower latitudes the largest variance is connected with intermediate frequency eastward traveling wave-5 and wave-6 with maxima at 40°N (Fig. 5b). Proceeding farther north, the peak values of eastward traveling waves shift to lower wavenumbers. At 70°N a low frequency westward traveling wave 1 is dominant (Fig. 5a). The spectra for spring are similar to winter. In summer at 40 and 50°N, the maximum variance of westward traveling waves is connected with higher wavenumbers than

Though not indicated to avoid confusion, lines of constant phase velocity at other latitudes would be identical to these. Units are gpm^2 and contour-lines are drawn for 50, 100, 200, 400, 600, 800, 1000, 1500, 2000, 2500, 3000, 3500, 4000, 4500 and 5000 gpm^2. The intervals between 50 and 100 gpm^2, between 600 and 800 gpm^2, and between 2000 and 2500 gpm^2 are stippled. These units differ from standard power spectral units (variance/frequency) in that they have been multiplied by frequency. A running average over three adjacent values results in non-zero contours at zero frequency. Values from 20°N are not included here because few exceeded 50 gpm^2.

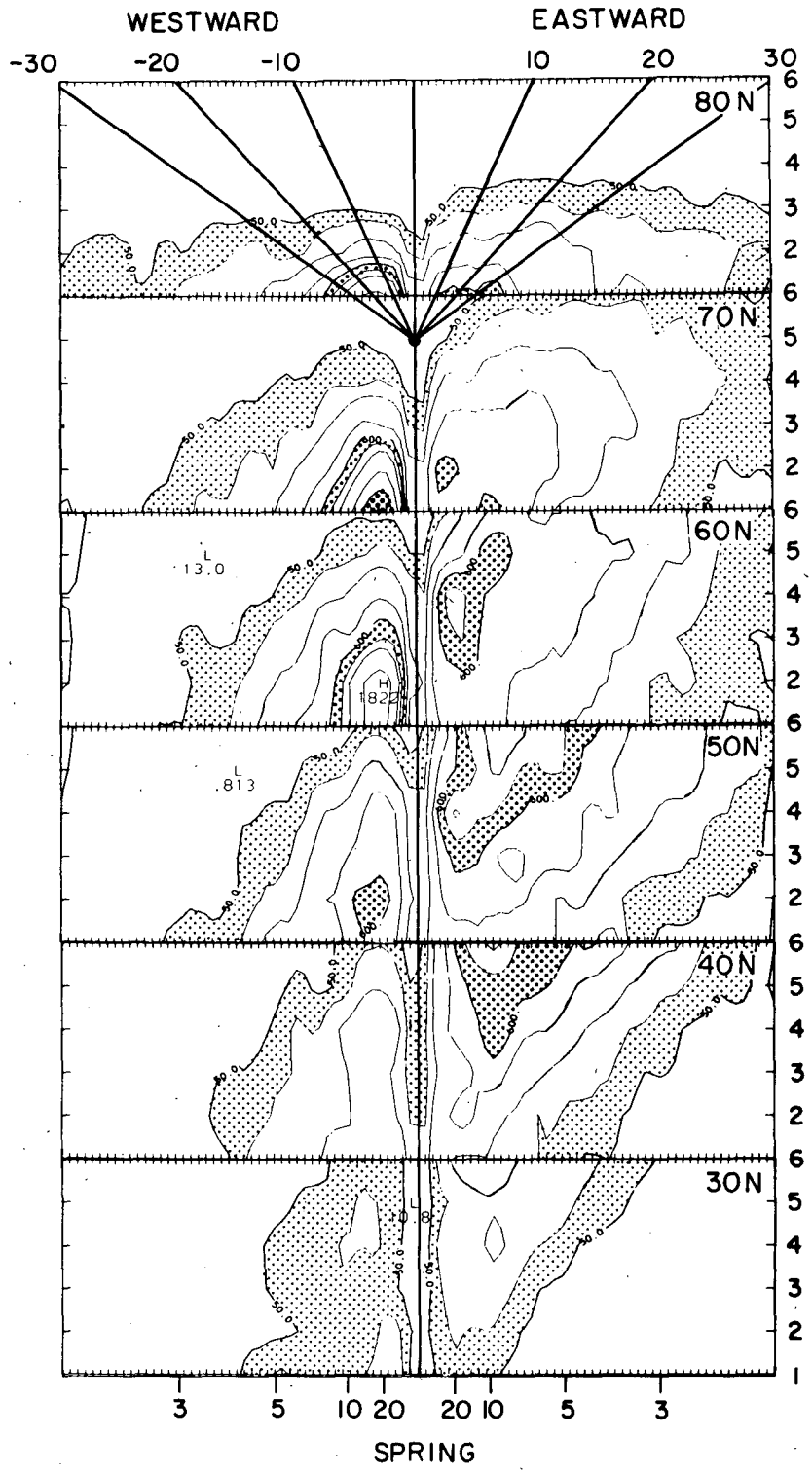

FIG. 2. As in Fig. 1, but for spring.

those of winter (Fig. 5c). The same is the case for eastward traveling waves north of 40°N. In fall at middle and high latitudes, large variance is indicated for intermediate frequency eastward traveling waves which is even larger than that of winter at 50 and 60°N (Fig. 5d).

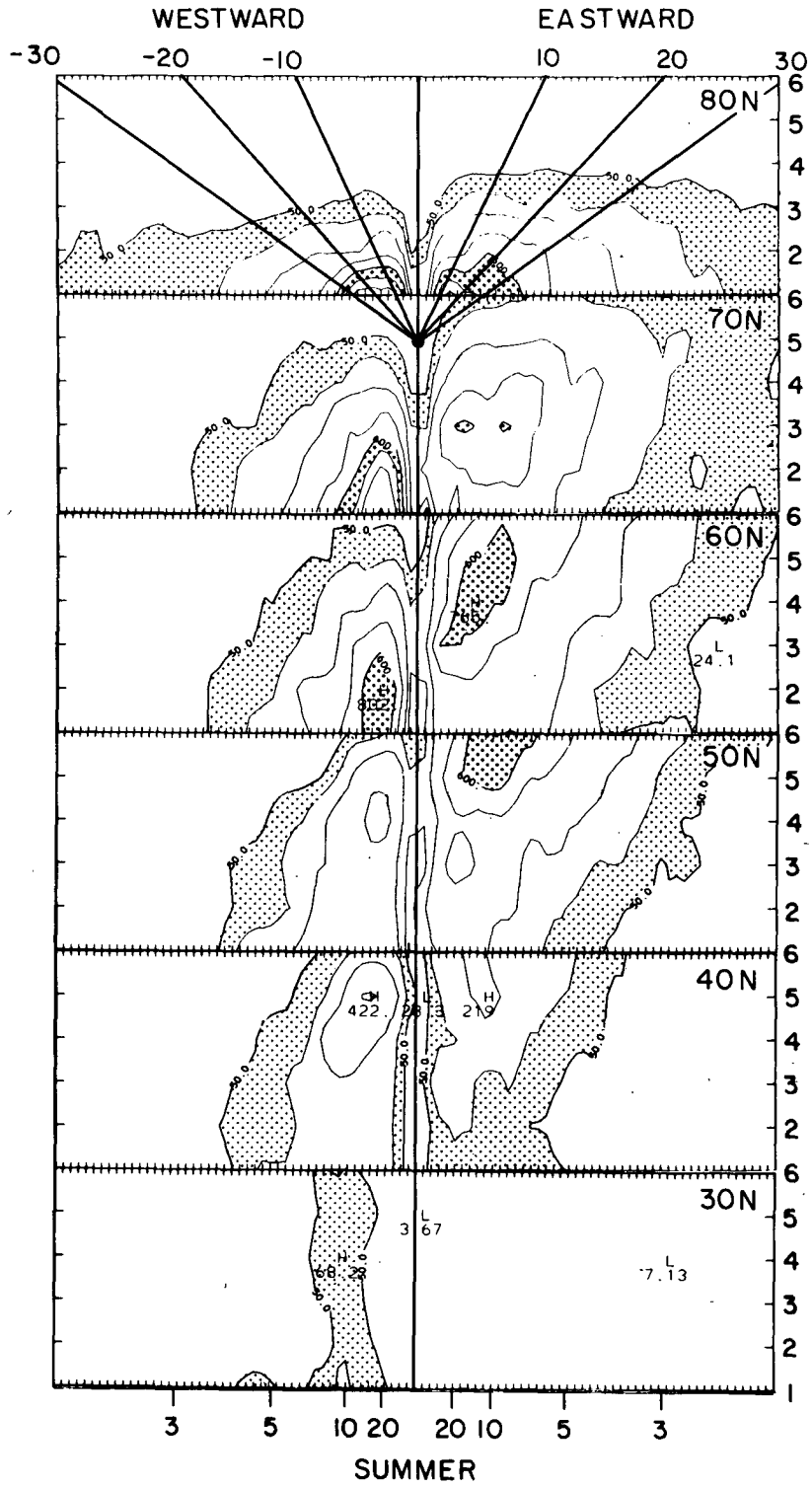

FIG. 3. As in Fig. 1, but for summer.

b. Frequency spectra for single wavenumbers

As mentioned at the beginning of this section details of some outstanding features will be discussed with the aid of frequency spectra for single wavenumbers. These frequency spectra illustrate for each wavenumber separately the same information contained in Figs. 1–4. In the interest of brevity, we show only

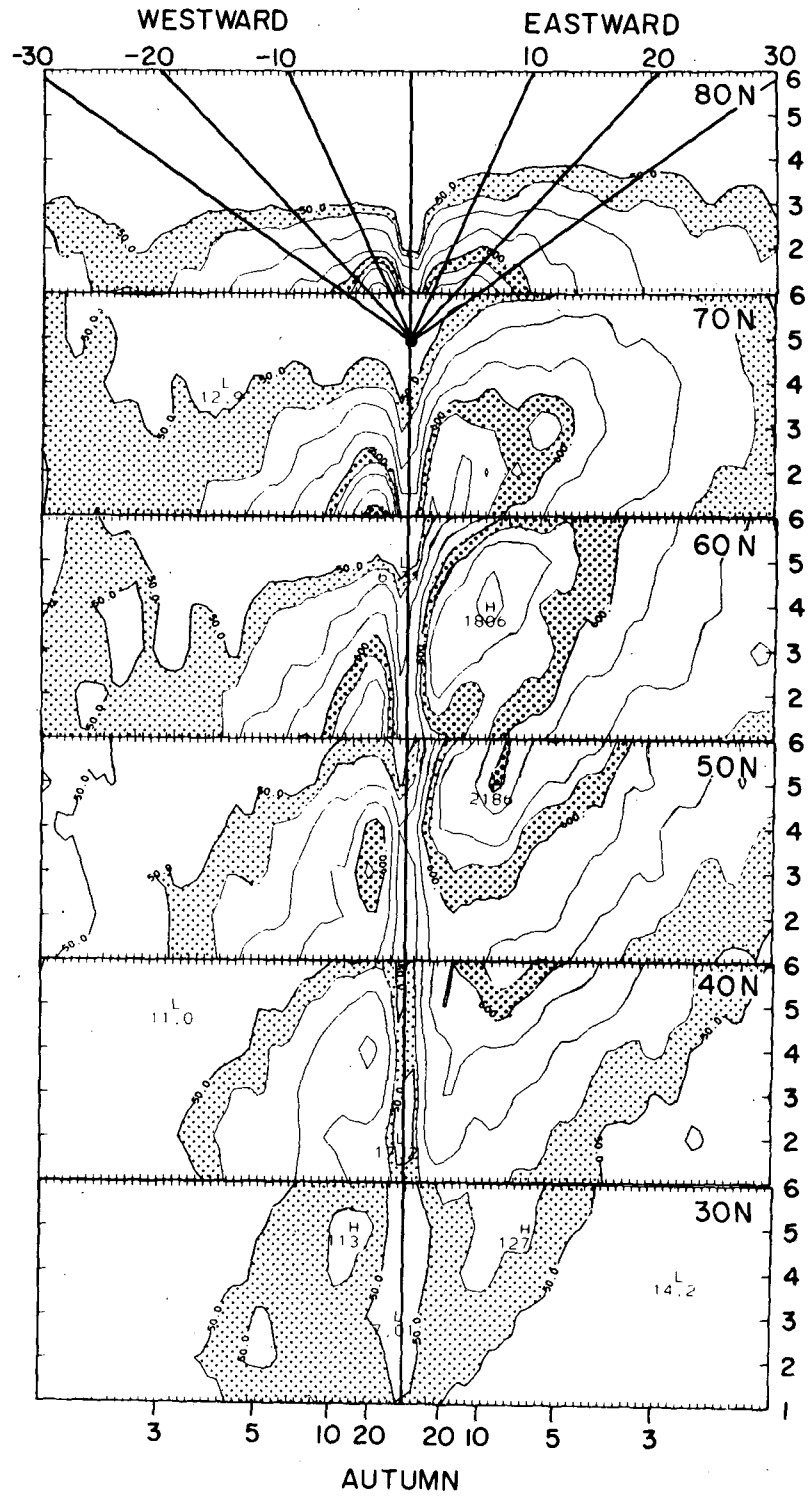

FIG. 4. As in Fig. 1, but for autumn.

winter and summer results in Figs. 6 and 7 and refer the reader to Figs. 2 and 4 for analogous spring and autumn results. Here, a linear power scale and logarithmic frequency scale is used which has the advantage that the area under each individual curve is proportional to the variance. The bandwidth is (2/96) cycles day^{-2}. When discussing Figs. 6 and 7, it must be pointed out that the scale of the ordinate varies

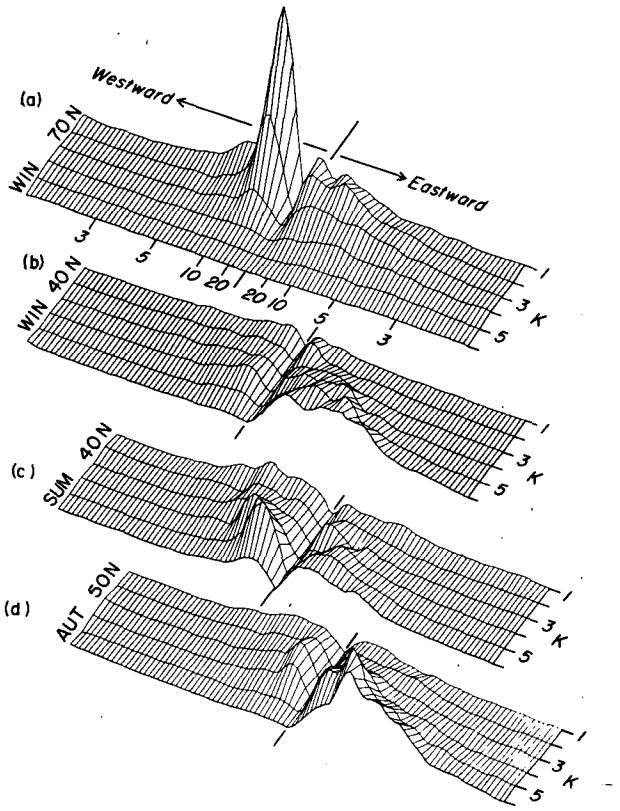

FIG. 5. Three-dimensional representation of the power of traveling waves for geopotential height at 250 mb. The abscissas represent frequencies as in Fig. 1, and K is the wavenumber. The vertical scale for summer is exaggerated by a factor of 2 as compared to winter and autumn. (a) Winter and 70°N; (b) winter and 40°N; (c) summer and 40°N; (d) autumn and 50°N.

from latitude to latitude and is different between wavenumbers 1 through 3 and wavenumbers 4 through 6.

The diagrams for wave-1 reveal that north of 50°N considerable westward propagating variance at periods between ~13 and 32 days (approximate half-power points) exists. There is a tendency for the peaks to be at shorter periods within this range in winter than during the other seasons (spring and autumn, not shown). In winter the same signal can also be recognized at 50°N. This low frequency westward propagating variance is largest at 70°N. We attribute these peaks to the 16-day wave (Kubota and Iida, 1954; Deland, 1965; Eliasen and Machenhauer, 1965, 1969; Boville, 1967; Arai, 1970; Sato, 1977; Madden, 1978; Ahlquist, 1982). Although in latitudes south of 50°N relative maxima are found in approximately the same period range (with a tendency for peaks to be shifted toward longer periods in winter and spring and towards shorter periods in summer and fall), the variance is much less there than at latitudes north of 50°N. For all seasons at 20, 30 and 40°N there are relative maxima in the westward variance with periods near five days which we attribute to the five-day wave (Deland, 1964; Eliasen and Machenhauer, 1965, 1969; Wallace and Chang, 1969; Madden and Julian, 1972; Misra, 1972). This is also the case for winter and spring at 50°N. For westward traveling wave 2, the spectra are similar to those of wave-1 north of 50°N for the low-frequency westward propagating variance. To some extent, this is also valid for wave-3. The fact that waves 1, 2 and 3 all have westward spectral peaks at a period near 16 days may mean that the longitudinal structure of the 16-day wave is not a simple sinusoid but, rather, a relatively local disturbance which results in several Fourier components. In the future, this will be investigated by using a more generalized technique of Hayashi (1979) to partition the local (rather than the zonal mean) power spectrum of transient waves consisting of multiple wavenumbers into standing and traveling parts, and by compositing techniques.

As mentioned in Section 3a, there is a large amount of variance connected with eastward traveling wave-5 and wave 6 at low and middle latitudes. This feature is discussed with the aid of results for wave 6. In this connection, wave-5 is similar to wave 6 in many respects. In winter at 30°N, there is a maximum in the eastward traveling variance for wave 6 centered at 13 days. A similar maximum is centered at five days at 50°N and both peaks are evident at 40°N. During the other seasons, only a single maximum is present. The resulting peaks are at 10 days, eight days, and seven days at 40°N in spring (not shown), at 50°N in summer, and at 50°N in autumn (not shown), respectively.

4. Discussion

We have highlighted relative maxima in westward propagating variance of wave 1 that are centered near five and 16 days in the last section. The latitudinal behaviors near these periods are summarized by plotting, in Fig. 8, the percentage of propagating variance around these maxima [$r(\phi)$] as a function of latitude ϕ, where $r(\phi)$ is

$$r(\phi) = \frac{\int_{f_1}^{f_2} \mathrm{PPUR}_\phi(f)\,d(\ln f)}{\int_{f=-0.5}^{f=+0.5} \mathrm{PPUR}_\phi(f)\,d(\ln f)}. \qquad (6)$$

For the five-day variance f_1 = 1/4.2 days and f_2 = 1/5.3 days, and for the 16-day variance f_1 = 1/13.7 days and f_2 = 1/24 days. From Fig. 8 we see that for the five day variance in winter $r(\phi)$ has a maximum at 20 and 30°N. The five day wave previously observed has been associated with the H_2^1 mode (Hough function H_n^m, where here m is the longitudinal wavenumber and $n - m$ relates to the latitudinal scale). This mode has a maximum near 50°N (*e.g.*, Longuet-

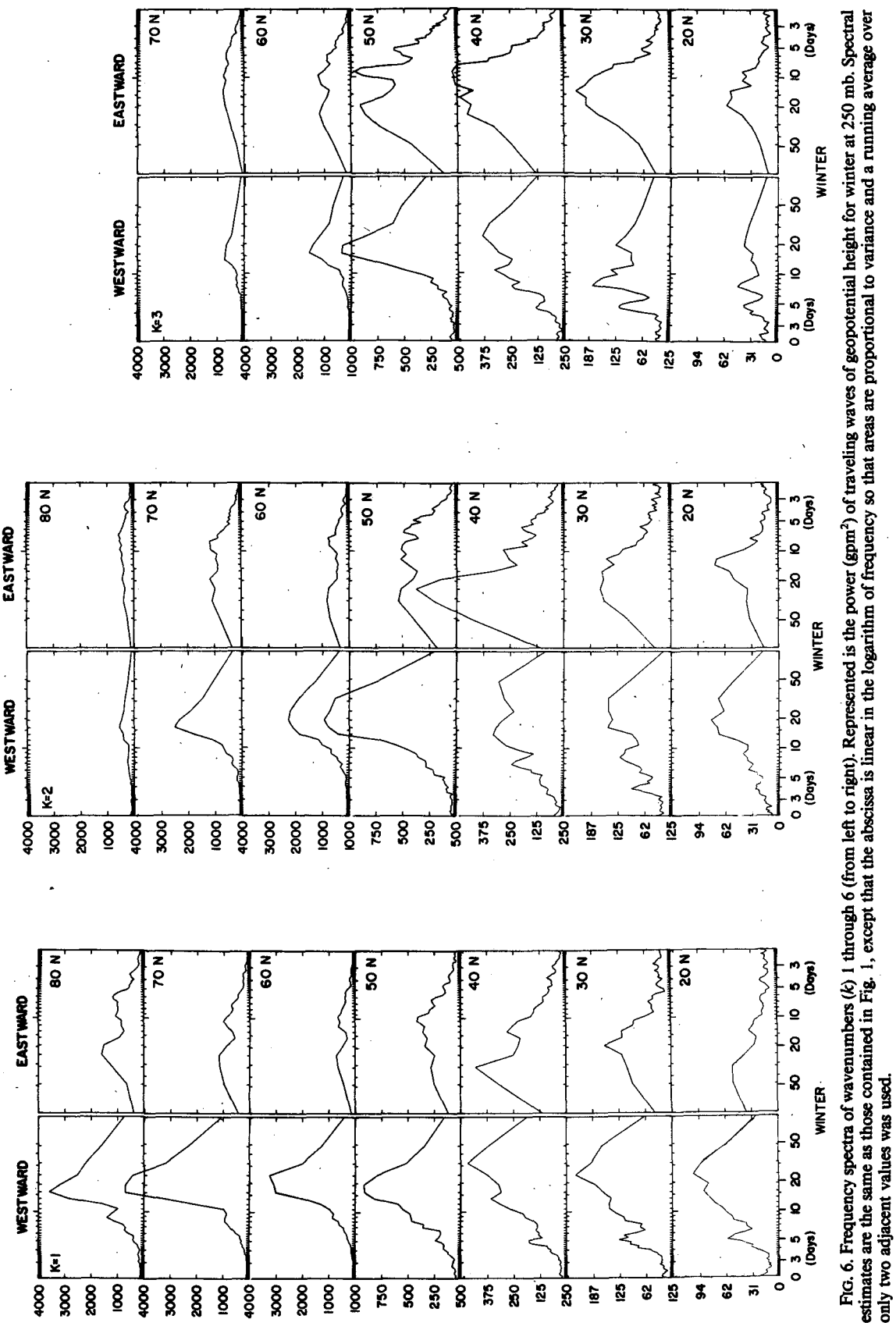

FIG. 6. Frequency spectra of wavenumbers (k) 1 through 6 (from left to right). Represented is the power (gpm^2) of traveling waves of geopotential height for winter at 250 mb. Spectral estimates are the same as those contained in Fig. 1, except that the abscissa is linear in the logarithm of frequency so that areas are proportional to variance and a running average over only two adjacent values was used.

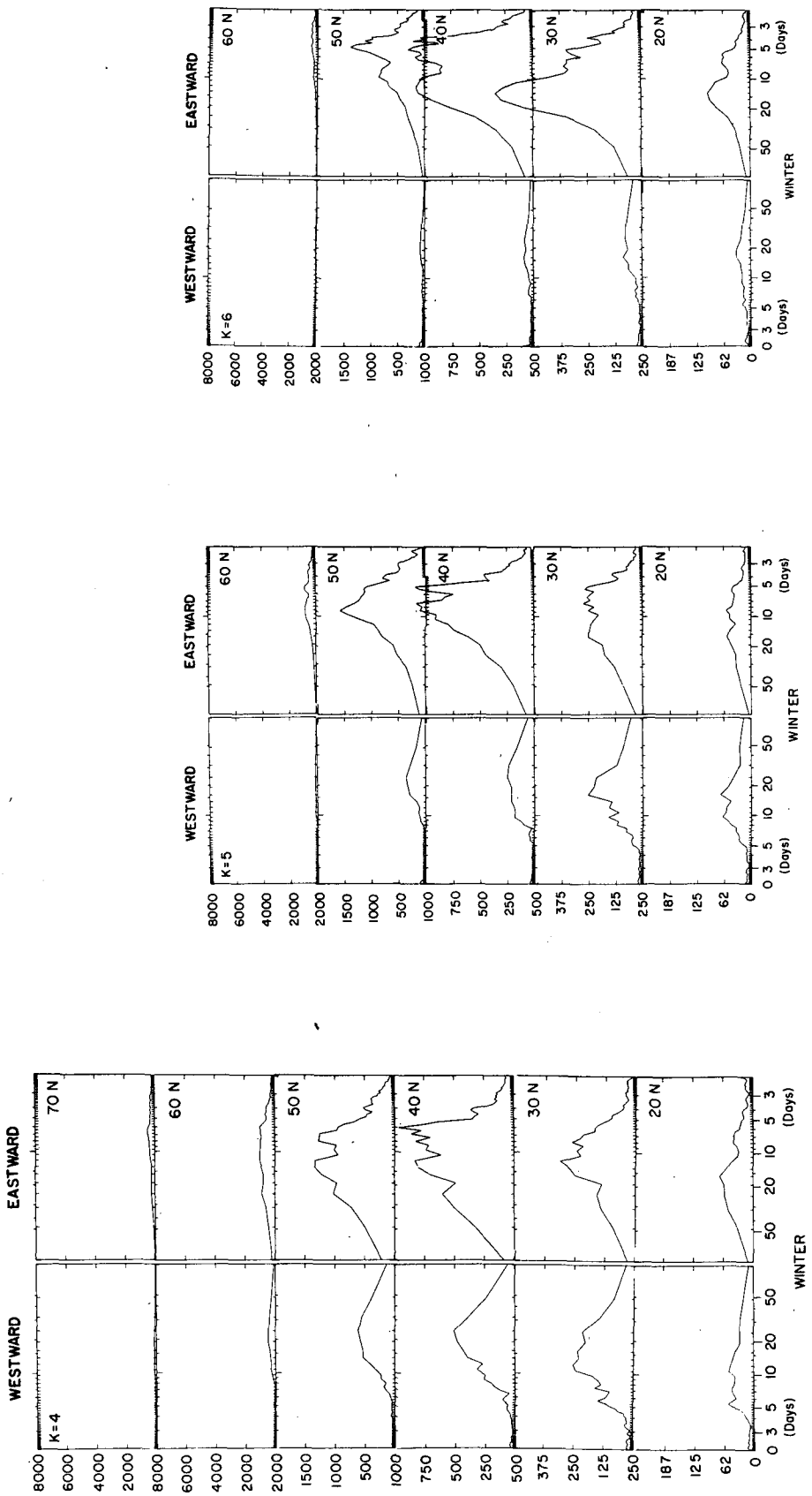

FIG. 6. (*Continued*)

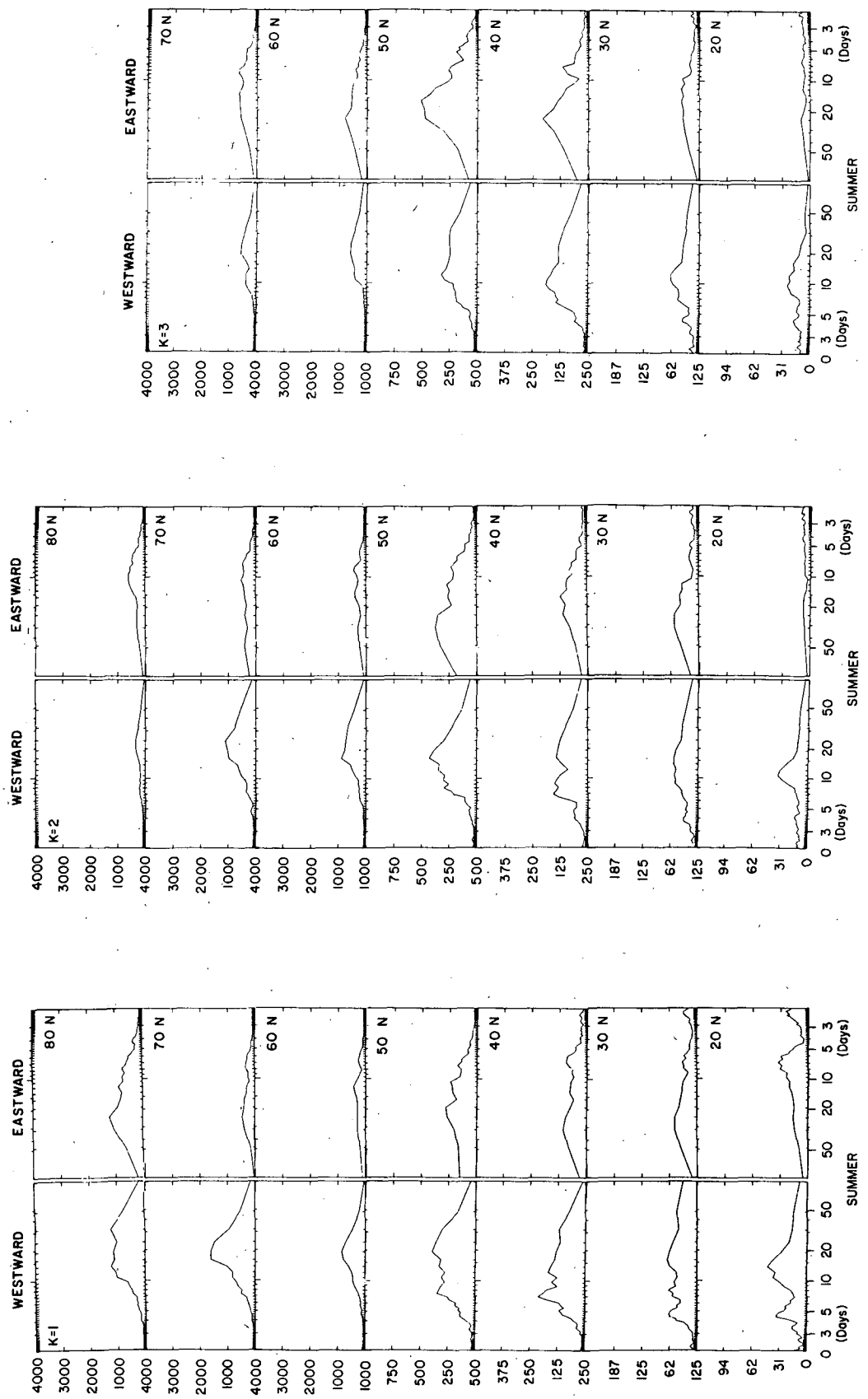

FIG. 7. As in Fig. 6, but for summer.

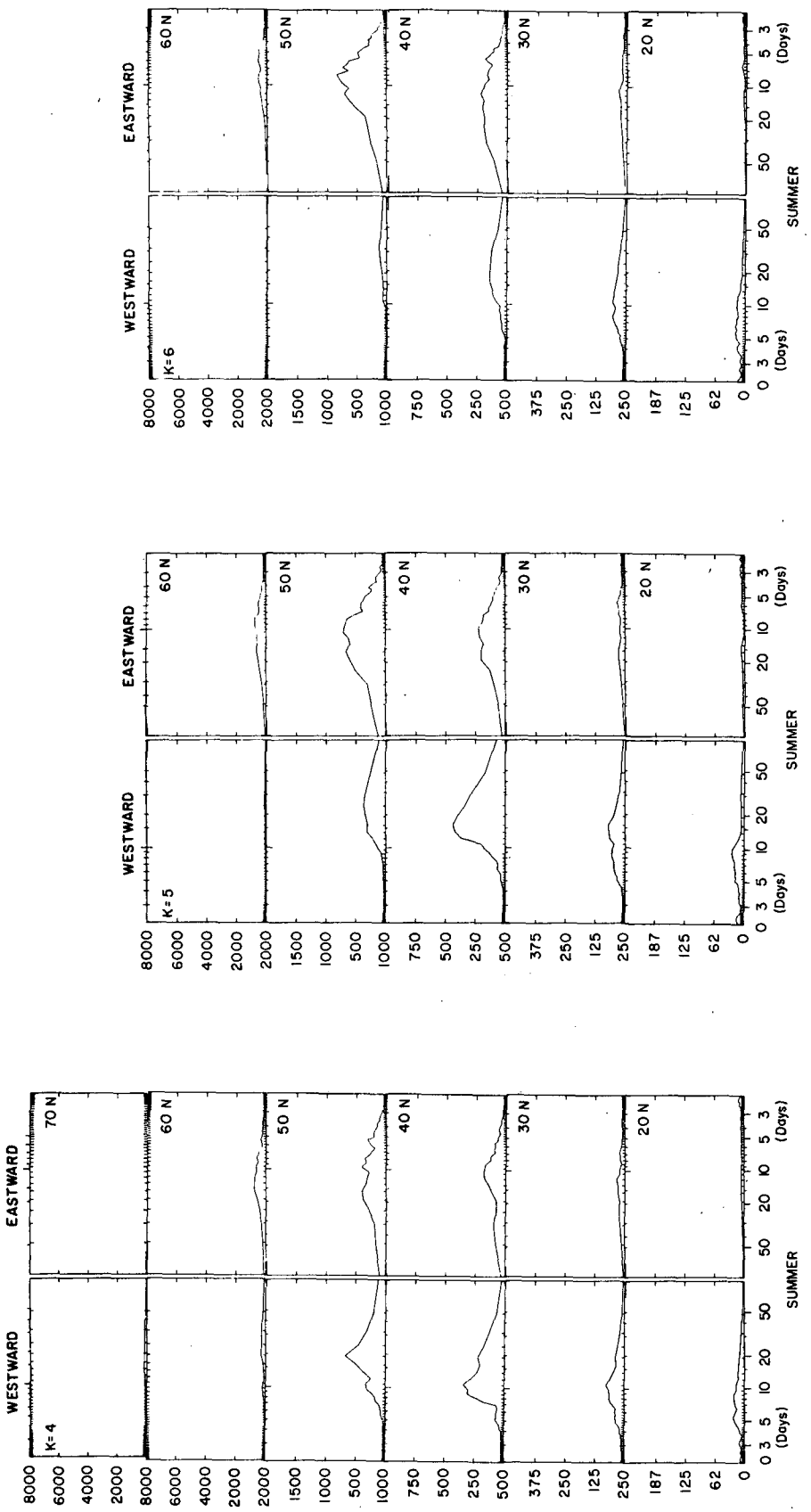

FIG. 7. (*Continued*)

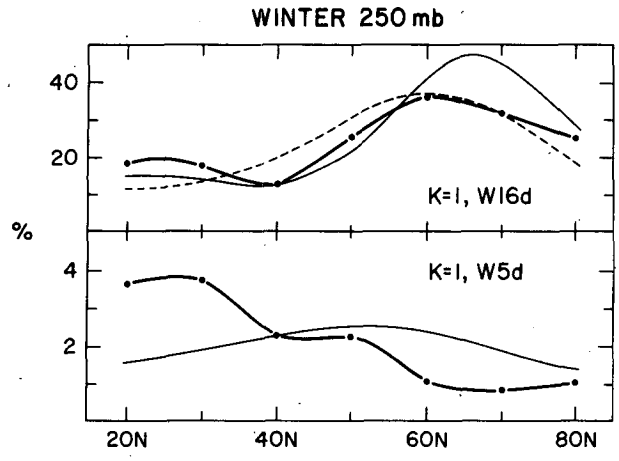

FIG. 8. Relative power (heavy solid lines with dots) of the westward propagating variance of wave 1 in frequency bands centered on 1/16 days (top) and 1/5 days (bottom) determined from (6) for winter. Thin solid lines represent the squared amplitudes of the H_4^1 (top), and H_2^1 (bottom), assuming an equivalent depth of 10 km for comparison. Thin dashed line is for the H_3^1 mode (top). Units for the squared amplitudes are arbitrary.

Higgins, 1968; Kasahara, 1976). Madden and Julian (1972) have suggested that, because total variance typically increases from lower to higher latitudes, the five-day wave may not stand out as clearly at high latitudes. In the same way the denominator of Eq. (6) increases from 20 to 80°N, effectively decreasing the percent variance associated with the five-day wave. It should also be noted that even at 20 and 30°N the variance between 4.2 and 5.3 days is only 4% of the total variance.

For the 16-day variance $r(\phi)$ has a primary maximum at 60°N and a secondary one at 20 and 30°N with a minimum at 40°N. This is qualitatively consistent with the H_4^1 mode which has a primary maximum near 60°N, a node near 35°N, and a secondary, out-of-phase maximum at 20°N. It is also consistent with the composite, 16-day wave structure determined by Madden (1978). For both the five and 16 day variances the quantity $r(\phi)$ is similar in all seasons.

Vertical behaviors of the variance in these two frequency bands at 30 and 70°N summarized in Fig. 9. Here, in order to compare directly with the external Rossby wave, we have plotted the quantity $A(p)$ as a function of pressure (p) where

$$A(p) = \left[2 \int_{f_1}^{f_2} \mathrm{PPUR}_p(f) d(\ln f)\right]^{1/2}, \qquad (7)$$

and f_1 and f_2 take on the values defined above. In Eq. (7) $A(p)$ is the amplitude of a simple sine wave with the same variance as that in the respective frequency bands. Because the magnitude of $A(p)$ is dependent on the limits of integration, its values in Fig. 9 cannot be taken as absolute estimates of wave amplitudes; but we expect that they reflect the relative behavior of those amplitudes in the vertical. For each season from 850 to 200 mb and again above 50 mb, the increase in the five-day variance is approximately what is expected of an external Rossby wave in an isothermal atmosphere [$a(p)$ from (1)]. Similar conclusions can be drawn for the 16-day variance in winter above ~400 mb and in spring and autumn above 70 mb. For the 16-day variance, the increase of $A(p)$ with height in the troposphere is faster than that of $a(p)$ in all seasons. Summer appears to be significantly different in that $A(p)$ decreases regularly in the stratosphere.

We speculate that some of the features of the vertical structures suggested in Fig. 9 result from changing evanescence of the waves in the presence of the effective index of refraction which is a function of both height and season. Evanescence is sensitive to the mean wind as measured in a coordinate system moving with the traveling wave. Large evanescence (rapid energy decrease) occurs in relative easterlies (Charney and Drazen, 1961; Dickinson, 1968) and may explain the difference in vertical growth rates between summer and winter for the 16-day wave in the stratosphere. For solstice conditions, Salby's (1981b) modeling work showed a similar difference above two scale heights for the H_1^4 mode. On the other hand, the five-day wave moves so rapidly westward that there may be no relative easterlies and therefore no large differences between winter and summer. Again Salby's (1981b) solstice results for the H_2^1 mode are nearly symmetric between winter and summer hemisphere below seven scale heights which

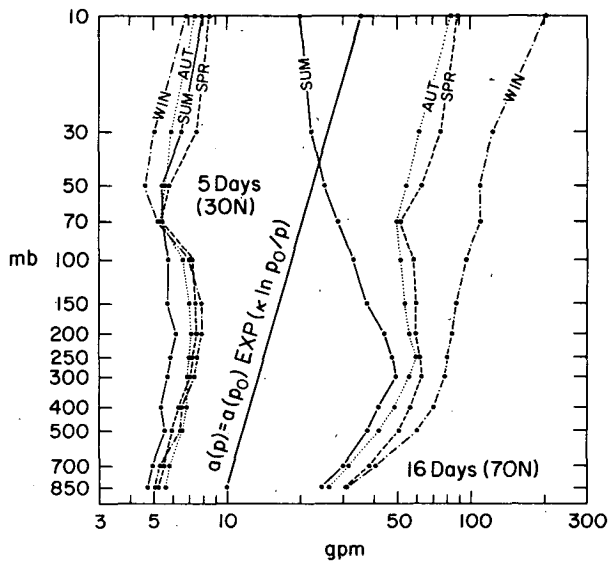

FIG. 9. The square root of twice the westward propagating variance of wave 1 in frequency bands centered on 1/16 days at 70°N (right-hand side) and 1/5 day at 30°N (left-hand side) for each season, determined from (7). Vertical structure of a Lamb wave is included for comparison.

is well above the uppermost level of Fig. 9. Evanescence also increases in the presence of poleward temperature gradients (Geisler and Dickinson, 1975; Salby, 1981a). This may be related to the amplitude decreases which begin near the tropopause (150 mb at 30°N for the five-day wave and 300-mb at 70°N for the 16-day wave).

Fig. 10 is similar to Fig. 8 but for eastward traveling wave-6 in winter. Here f_1 = 1/5.3 days and f_2 = 1/4.4 days for the five-day eastward variance and f_1 = 1/19.2 days and f_2 = 1/10.7 days for the 13-day eastward variance. These two bands were selected in order to examine the two corresponding peaks in Fig. 6. It is seen from Fig. 10 that there is a relative maximum in the percent variance contained in the five-day band at 50°N and one in the 13-day band at 30°N. For bands centered on the frequencies of the peaks evident in the spectra for wave-6 in other seasons as described in Section 3b, the profiles of $r(\phi)$ are similar to that of the 13-day variance in Fig. 10 except the relative maxima occur at 40°N in spring and 50°N in summer and autumn.

Fig. 11 shows that $A(p)$ for the five and 13-day eastward variance in winter has distinct maxima at 300 mb and between 250 and 200 mb, respectively. For other seasons $A(p)$ is very similar to that for the 13-day variance in Fig. 11.

Fig. 11 suggests that the vertical structures of the disturbances responsible for the wave-6 eastward propagating variance are far different from those of external Rossby waves. We tentatively conclude that they may draw their energy from baroclinic or barotropic instabilities. For example, the five day wave-6 eastward variance may be related to the baroclinically unstable traveling waves that Hartmann (1974) has argued are responsible for spectral peaks that he has found in a 13-year winter record of rawinsonde data from Ocean Weather Ships C (53°N, 35°W) and D

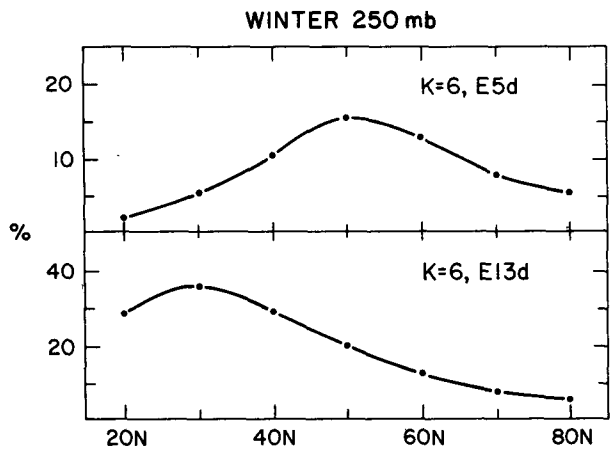

FIG. 10. As in Fig. 8, but for eastward propagating variance of wave 6 in frequency bands centered on 1/5 day (top) and 1/13 day (bottom) for winter. No model is included for comparison.

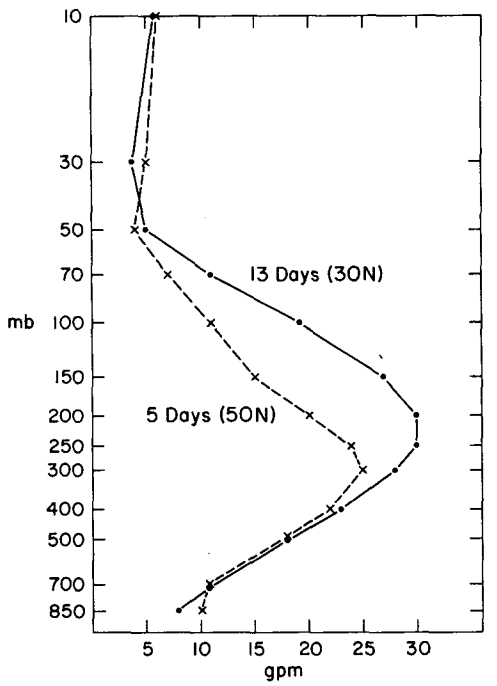

FIG. 11. As in Fig. 9, but for eastward propagating variance of wave 6 in the frequency band centered on 1/5 day at 50°N and in the frequency band 1/13 day at 30°N for winter only.

(44°N, 41°W). In addition, Salby (1982) and Hamilton (1983) have documented an eastward propagating wave 5 of similar structure and 8–15 day period in the Southern Hemisphere. Salby tentatively identified this wave with a baroclinically unstable mode as well.

5. Summary and outlook

We have used space–time spectral analyses in order to isolate large-scale traveling waves. We have discussed only a small part of the results and emphasized westward propagating wave 1 and eastward traveling wave-6. Since the amplitude of traveling variance is large, it is important to know more about the behavior of the responsible disturbances. We plan to do further work to learn more of the nature and effects of these disturbances, and of other disturbances responsible for additional propagating variance displayed in Section 3 but not specifically discussed.

Acknowledgments. We wish to acknowledge the help of the NCAR Computing Facility and Graphics Department. R. Jenne and W. Spangler provided the data in an easily accessible format. We were also fortunate in receiving several thoughtful comments from the anonymous reviewers which helped to improve the manuscript.

REFERENCES

Alquist, J. E., 1982: Normal-mode global Rossby waves: Theory and observations. *J. Atmos. Sci.*, **39**, 193–202.

Arai, Y., 1970: A statistical study of ultralong waves. *J. Meteor. Soc. Japan,* **48,** 469–478.

Boville, B. W., 1967: Planetary waves in the stratosphere and their upward propagation. *Space Res.,* **7,** 20–29.

Charney, J. G., and P. J. Drazin, 1961: Propagation of planetary-scale disturbances from the lower into the upper atmosphere. *J. Geophys. Res.,* **66,** 83–109.

Deland, R. J., 1964: Traveling planetary waves. *Tellus,* **16,** 271–273.

——, 1965: Some observations of the behavior of spherical harmonic waves. *Mon. Wea. Rev.,* **93,** 307–312.

Dickinson, R. E., 1968: Planetary Rossby waves propagating vertically through weak westerly wind wave guides. *J. Atmos. Sci.,* **25,** 984–1002.

Eliasen, E., and B. Machenhauer, 1965: A study of the fluctuations of atmospheric planetary flow patterns represented by spherical harmonics. *Tellus,* **17,** 220–238.

——, and ——, 1969: On the observed large-scale atmospheric wave motions. *Tellus,* **21,** 149–165.

Fraedrich, K., and H. Böttger, 1978: A wavenumber-frequency-analysis of the 500 mb geopotential at 50°N. *J. Atmos. Sci.,* **35,** 745–750.

Garcia, R. R., and J. E. Geisler, 1981: Stochastic forcing of small amplitude oscillations in the stratosphere. *J. Atmos. Sci.,* **38,** 2187–2197.

Geisler, J., and R. E. Dickinson, 1975: External Rossby modes on a β-plane with realistic vertical wind shear. *J. Atmos. Sci.,* **32,** 2082–2093.

——, and ——, 1976: The five-day wave on a sphere with realistic zonal winds. *J. Atmos. Sci.,* **33,** 632–641.

Hamilton, K., 1983: Aspects of wave behavior in the mid and upper troposphere of the Southern Hemisphere. *Atmos.-Ocean.,* **21,** 40–54.

Hartmann, D., 1974: Time spectral analysis of midlatitude disturbances. *Mon. Wea. Rev.,* **102,** 348–362.

Haurwitz, B., 1937: The oscillations of the atmosphere. *Gerlands Beitr. Geophys.,* **51,** 195–233.

——, 1940a: The motion of atmospheric disturbances. *J. Mar. Res.,* **3,** 35–50.

——, 1940b: The motion of atmospheric disturbances on a spherical earth. *J. Mar. Res.,* **3,** 254–267.

Hayashi, Y., 1974: Spectral analysis of tropical disturbances appearing in a GFDL General Circulation Model. *J. Atmos. Sci.,* **31,** 180–218.

——, 1977: On the coherence between progressive and retrogressive waves and a partition of space-time power spectra into standing and traveling parts. *J. Appl. Meteor.,* **16,** 368–373.

——, 1979: A generalized method of resolving transient disturbances into standing and traveling waves by space-time spectral analysis. *J. Atmos. Sci.,* **36,** 1017–1029.

——, 1982: Space-time spectral analysis and its applications to atmospheric waves. *J. Meteor. Soc. Japan (Centennial Issue),* **60,** 156–171.

——, and D. G. Golder, 1977: Space-time spectral analysis of midlatitude disturbances appearing in a GFDL General Circulation Model. *J. Atmos. Sci.,* **34,** 237–262.

Hirota, I., 1971a: Excitation of planetary Rossby waves in the winter stratosphere by periodic forcing. *J. Meteor. Soc. Japan,* **49,** 439–449.

——, 1971b: On the response of forced Rossby waves to the time change of zonal wind and forcing. *J. Meteor. Soc. Japan,* **49,** 545–552.

Holton, J. R., 1975: *The Dynamic Meteorology of the Stratosphere and Mesosphere. Meteor. Monogr.,* No. 37, Amer. Meteor. Soc., 218 pp.

Hough, S. S., 1898: On the application of harmonic analysis to the dynamical theory of tides. II: On the general integration of Laplace's dynamical equations. *Phil. Trans. Roy. Soc. London,* **A191,** 139–185.

Jenne, R. L., 1975: Data sets for meteorological research. NCAR Tech. Note TN/IA, 111, 172 pp. [NTIS PB 246564/AS].

Kao, S.-K., 1970: Wavenumber-frequency spectra of temperature in the free atmosphere. *J. Atmos. Sci.,* **27,** 1000–1007.

——, and C. N. Chi, 1978: Mechanism for the growth and decay of long- and synoptic-scale waves in the mid-troposphere. *J. Atmos. Sci.,* **35,** 1375–1387.

Kasahara, A., 1976: Normal modes of ultralong waves in the atmosphere. *Mon. Wea. Rev.,* **104,** 669–690.

Kubota, S., and M. Iida, 1954: Statistical characteristics of the atmospheric disturbances. *Pap. Meteor. Geophys.,* **5,** 22–34.

Lamb, H., 1932: *Hydrodynamics.* Dover, 738 pp.

Longuet-Higgins, M. S., 1968: The eigenfunction of Laplace's tidal equations over a sphere. *Phil. Trans. Roy. Soc. London,* **A262,** 511–607.

Madden, R. A., 1978: Further evidence of traveling planetary waves. *J. Atmos. Sci.,* **35,** 1605–1618.

——, and P. R. Julian, 1972: Further evidence of global-scale 5-day pressure waves. *J. Atmos. Sci.,* **29,** 1464–1469.

Margules, M., 1893: Luftbewegungen in einer rotierenden Sphäroidschale, II. *Sitzungsber. Akad. Wiss. Wien, Math-Naturwiss. Kl., Abt. 2a,* **102,** 11–56. [English translation by Haurwitz, 1980: NCAR/TN-156+STR].

Misra, B. M., 1972: Planetary pressure wave of 4- to 5-day period in the tropics. *Mon. Wea. Rev.,* **100,** 313–316.

Pratt, R. W., 1976: The interpretation of space-time spectral quantities. *J. Atmos. Sci.,* **33,** 1060–1066.

——, and J. M. Wallace, 1976: Zonal propagation characteristics of large-scale fluctuations in the midlatitude troposphere. *J. Atmos. Sci.,* **33,** 1184–1194.

Rossby, C.-G., 1949: On the dispersion of planetary waves in a barotropic atmosphere. *Tellus,* **1,** 54–58.

——, *et al.* 1939: Relations between variations in the intensity of the zonal circulation of the atmosphere and the displacements of the semipermanent centers of action. *J. Mar. Res.,* **2,** 38–55.

Salby, M., 1981a: Rossby normal modes in nonuniform background configurations. Part I: Simple fields. *J. Atmos. Sci.,* **38,** 1803–1826.

——, 1981b: Rossby normal modes in nonuniform background configurations. Part II: Equinox and solstice conditions. *J. Atmos. Sci.,* **38,** 1827–1840.

——, 1982: A ubiquitous wave 5 anomaly in the Southern Hemisphere during FGGE. *Mon. Wea. Rev.,* **110,** 1712–1720.

Sato, Y., 1977: Transient planetary waves in the winter stratosphere. *J. Meteor. Soc. Japan,* **55,** 89–105.

Schäfer, J., 1979: A space-time analysis of tropospheric planetary waves in the Northern Hemisphere. *J. Atmos. Sci.,* **36,** 1117–1123.

Schoeberl, M. R., and J. H. E. Clark, 1980: Resonant planetary waves in a spherical atmosphere. *J. Atmos. Sci.,* **37,** 20–28.

Speth, P., and E. Kirk, 1981: A one-year study of power spectra in wavenumber–frequency domain. *Beitr. Phys. Atmos.,* **54,** 186–206.

Tsay, C-Y., 1974: Analysis of large scale wave disturbances in the tropics simulated by an NCAR Global Circulation Model. *J. Atmos. Sci.,* **31,** 330–339.

Wallace, J. M., and C.-P. Chang, 1969: Spectrum analysis of large scale wave disturbances in the tropical lower troposphere. *J. Atmos. Sci.,* **26,** 1010–1025.

Zangvil, A., and M. Yanai, 1980a: Upper tropospheric waves in the tropics. Part I: Dynamical analysis in the wavenumber–frequency analysis. *J. Atmos. Sci.,* **37,** 283–298.

——, and ——, 1980b: Upper tropospheric waves in the tropics. Part II: Association with clouds in the wavenumber-frequency domain. *J. Atmos. Sci.,* **38,** 232–253.